PAPER • OPEN ACCESS

Prethermalization and dynamic phase transition in an isolated trapped ion spin chain

To cite this article: Zhe-Xuan Gong and L-M Duan 2013 *New J. Phys.* **15** 113051

Prethermalization and dynamic phase transition in an isolated trapped ion spin chain

Zhe-Xuan Gong[1,2,4] **and L-M Duan**[1,3]

[1] Department of Physics, University of Michigan, Ann Arbor, MI 48109, USA
[2] Joint Quantum Institute, University of Maryland Department of Physics and National Institute of Standards and Technology, College Park, MD 20742, USA
[3] Center for Quantum Information, IIIS, Tsinghua University, Beijing 100084, People's Republic of China
E-mail: gzx@umich.edu

Abstract. We propose an experimental scheme to observe prethermalization and a dynamic phase transition in a one-dimensional XY spin chain with long-range interactions and inhomogeneous lattice spacing, which can be readily implemented with a recently developed trapped-ion quantum simulator. Local physical observables are found to relax to prethermal values at an intermediate timescale, followed by complete relaxation to thermal values at much longer time. The physical origin of prethermalization is shown to result from a non-trivial structure in the lower half of the energy spectrum. The dynamic behavior of the system is shown to cross different phases when the interaction range is continuously tuned, indicating the existence of a dynamic phase transition.

[4] Author to whom any correspondence should be addressed.

IOP Institute of Physics Φ DEUTSCHE PHYSIKALISCHE GESELLSCHAFT

Contents

The dynamic properties of isolated quantum many-body systems have garnered intense interest in recent years [1, 2]. On the theory side, research has been centered on whether and how an isolated quantum system approaches thermal equilibrium. While certain observables are found to relax to equilibrium in some large systems [3–7], it remains unclear under what conditions and on which timescale equilibration occurs in generic systems [8–11]. On the experimental side, recent progress with cold atoms [12–14] and trapped ions [15–20] has made it possible to simulate well controlled simple models, such as the one-dimensional (1D) Bose gas and transverse field Ising model. These quantum systems can be well isolated from the environment and have long coherence times, and their physical properties can be measured at the single-atom level, providing an unprecedented opportunity for studying non-equilibrium dynamics in closed interacting systems.

A particularly intriguing phenomenon in this context is *prethermalization* [21], which has been shown to emerge in various theoretical setups [22–24], and has been experimentally observed in ultracold atomic gas [14]. Prethermalization is characterized by the establishment of a quasi-stationary state at an intermediate timescale, followed by relaxation to a stationary state at a much longer timescale (thermalization). The physical origin of prethermalization, however, is still elusive, and is speculated to be related to the quasi-integrability of the model [14, 23].

In this paper, we propose a new experimental scheme for observing and studying prethermalization and a related dynamic phase transition in an XY spin model, which can be implemented with the current trapped-ion quantum simulator of [19]. Our model features long-range spin–spin interaction and an inhomogeneous lattice spacing, and unlike many other systems, the prethermalization can occur already for as few as a dozen spins, allowing for its observation in current experimental systems. The prethermalization found in this system results from a non-trivial structure in the energy spectrum, which in turn arises due to a combination of long-range interaction and inhomogeneous lattice spacing. In addition, by tuning the range of interactions with an experimental knob, we find that the dynamic behavior of this system exhibits three different phases: thermalization only, prethermalization followed by thermalization and prethermalization only. The transition between these different phases becomes sharper with an increasing number of spins, hinting at the existence of a dynamic phase transition [25] in the thermodynamic limit.

1. Model and its dynamics

Our spin model is based on the experimental system of a chain of ions confined in a linear Paul trap (figure 1). Through proper configuration of the Raman beams, the optical dipole force can
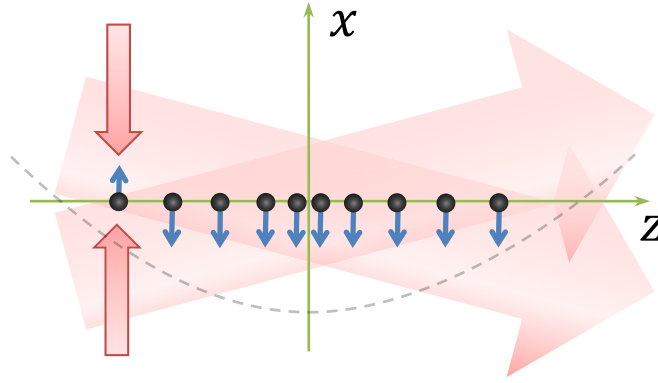
Figure 1. Schematic view of the proposed experimental setup: a chain of N ions are trapped along the z direction in a 1D harmonic linear Paul trap. The global Raman beams generate a spin-dependent force along the x direction, resulting in effective Ising-type interaction. To induce the dynamics, a focused laser beam is applied on one end of the ion chain to selectively flip only the first spin.

generate an effective transverse field Ising model [16, 17, 26]

$$H = \sum_{i<j}^{N} J_{i,j}\sigma_i^x\sigma_j^x + B\sum_{i=1}^{N}\sigma_i^z, \tag{1}$$

where σ_i is the spin-1/2 Pauli matrix for the ith ion qubit. The interaction coefficients J_{ij} in equation (1) are given by

$$J_{i,j} = \Omega^2 \sum_{m=1}^{N} \frac{\eta_{i,m}\eta_{j,m}\omega_m}{\mu^2 - \omega_m^2},$$

where μ is the Raman beatnote frequency, Ω is the effective Rabi frequency, which is assumed to be the same for all of the ions, $\{\omega_m\}$ are the phonon mode frequencies of the ions in the x direction and $\eta_{i,m}$ are the Lamb–Dicke parameters measuring the coupling between the ith ion and the mth phonon mode. We are interested in the region where $B \gg \max\{J_{ij}\}$. In this limit, the $\sigma_i^+\sigma_j^+$ and $\sigma_i^-\sigma_j^-$ terms in equation (1) will be energetically forbidden, and we end up with the XY Hamiltonian

$$H \approx H_{XY} = \sum_{i<j} 2J_{i,j}(\sigma_i^+\sigma_j^- + \text{h.c.}) + B\sum_i \sigma_i^z. \tag{2}$$

A unique feature of the Hamiltonians (1) and (2) realized with the ion system is that the interaction characterized by J_{ij} is long ranged, and the interaction range is readily tuned by changing the beatnote frequency μ. In particular, in a range of μ, J_{ij} can be roughly approximated by a power-law decay with $J_{ij} \sim |i-j|^{-\alpha}$, where α varies from 0 to 3 when we tune μ [19]. In the following analysis, for a given μ, we fit the coefficient J_{ij} with $J_{ij} \sim |i-j|^{-\alpha}$ and use the fitting parameter α as an indicator of the range of interaction.

The $1/r^\alpha$ Ising model (equation (1)) with no transverse field (essentially classical) can be analytically solved [27, 28]. Its dynamic properties have also been recently studied in [24, 29], where it is found that if α is smaller than the dimensionality of the system, the total interaction energy per site diverges, drastically changing the dynamics after a global quantum

quench, with possible emergence of prethermalization. However, the long range XY model (equation (2)) contains non-commuting terms and is generally not exactly solvable, making its dynamic properties largely unknown. Here, we consider a particularly interesting setup that shows rich dynamic properties and is practical for experimental demonstration. We first initialize all of the spins through optical pumping to the spin down state with $\sigma_i^z = -1$, which is an eigenstate of H_{XY} and hence stationary. We then use a focused laser beam to flip the first spin (left end ion) to $\sigma_i^z = 1$ (see figure 1). The starting state $|\psi(0)\rangle = |\uparrow\downarrow\downarrow\cdots\downarrow\rangle$ is no longer an eigenstate of H_{XY}, and is subject to the dynamics with $|\psi(t)\rangle = e^{iH_{XY}t/\hbar}|\psi(0)\rangle$. We consider the time evolution of the local observables $\langle\sigma_i^z(t)\rangle$ and their correlations $\langle\sigma_i^z(t)\sigma_j^z(t)\rangle$, which can be directly measured in the experiments. For convenience of description of the dynamics, we introduce the operator

$$C = \sum_{i=1}^{N} f_i \frac{\sigma_i^z + 1}{2},$$

where the coefficients $f_i \equiv (2i - N - 1)/(N - 1)$ are equally distributed between $[-1, 1]$ from $i = 1$ to N. The expectation value of C varies between $[-1, 1]$, and physically measures the relative position of the spin excitation. It is easy to check that $\langle\psi(0)|C|\psi(0)\rangle = -1$, meaning that the spin excitation is initially at the left edge of the chain. We also note that for any state with spatial inversion symmetry around the center of the chain, $\langle C \rangle = 0$.

2. Prethermalization and dynamic phase transition

To explore the dynamic behavior, we first perform numerical calculations by using exact diagonalization of an $N = 16$ ion chain, which corresponds to the current size of the experimental trapped ion quantum simulator in [19]. As shown in figure 2, we choose two parameter settings with the corresponding fitting parameter $\alpha \approx 2.6$ and 0.52, which represent, respectively, the short-range and the long-range interactions. The distributions of the exact coupling coefficients J_{ij} are shown in figure 2 for these two cases. Note that our calculation is based on the approximated XY Hamiltonian (equation (2)). However, we have numerically verified that the relative differences of the calculated $\langle C \rangle$ and $\langle\sigma_i\sigma_j\rangle$ obtained by solving the original transverse field Ising Hamiltonian (equation (1)) are negligible at all times ($<10^{-3}$) when $B > 1000J_0$. It is worth mentioning that the error caused by the non-$\sum_i \sigma_i^z$-conserving terms from the finite B field does not accumulate over time: the population of our state outside of the single excitation subspace can be estimated as $\epsilon \sim \sum_{i,j}(J_{ij}/B)^2$, which is independent of time and can be made arbitrarily small by choosing a sufficiently large B. In practice, as $J_0 \sim \Omega(\eta_x/N)(\eta_x\Omega)/(\mu - \omega_x)$, and a trapped ion quantum simulator requires $\eta_x \ll 1$ and $\eta_x\Omega \ll \mu - \omega_x$ [26], $\Omega > 1000J_0$ is typical for $N > 10$ ions (see [19] and also example parameters in figure 2). Since the transverse magnetic field is generated by a resonant carrier transition [16, 17], by splitting the Raman laser power evenly between the two sidebands alongwith the carrier transition, $B > 1000J_0$ can be readily achieved. Moreover, ϵ decreases with increasing N, as the J_{ij} will scale down faster than $1/N$ for a given laser power [30].

For these choices of parameters, the short-time dynamics with $t \in [0, 2/J_0]$ for $\langle C \rangle$ is shown in figures 3(a) and (b). In the short-range interaction case, we observe that the spin excitation, initially located at the left edge of the chain, travels almost coherently to the other side and oscillates back and forth with relatively small dispersion. In contrast, in the long-range
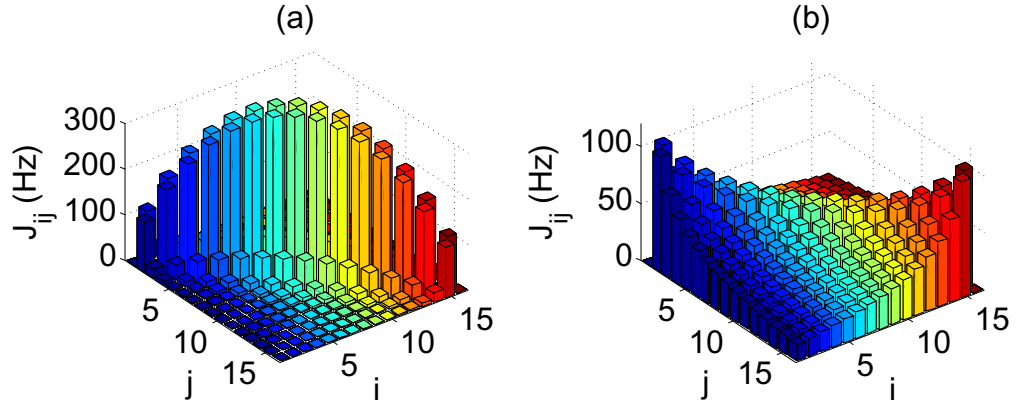
Figure 2. (a) Distribution of J_{ij} for short-range interactions with the beatnote frequency set at $\mu = 5.2\,\text{MHz}$, a trap frequency in the z direction of $\omega_z = 100\,\text{kHz}$, and $\eta_x \Omega = 40\,\text{kHz}$. The corresponding fitting parameter $\alpha \approx 2.6$ in this case. (b) Distribution of J_{ij} for long-range interactions with $\mu = 5.02\,\text{MHz}$, $\omega_z = 600\,\text{kHz}$, $\eta_x \Omega = 3.9\,\text{kHz}$, and the corresponding fitting parameter $\alpha \approx 0.52$. In both cases we choose a trap frequency in the x direction of $\omega_x = 5\,\text{MHz}$ and average interaction strength $J_0 = \sum_{i \neq j} J_{ij}/N^2 = 20\,\text{Hz}$. Note that all of the frequencies here are angular frequencies.

interaction case, the spin excitation diffuses and somehow gets locked before it reaches the middle of the chain (with $\langle C \rangle \approx -0.4$).

To clarify the long-time dynamics, we use the finite-time-averaged quantity $\overline{A(t)}$, defined as $\overline{A(t)} \equiv \frac{1}{t} \int_0^t \langle A(\tau) \rangle \, d\tau$ for the observable A [31, 32], thereby averaging out temporal fluctuations on short time scales (the following dynamic behaviors are qualitatively the same even without performing any time averaging). The long-time dynamics is shown in figures 3(c) and (d). In the short-range interaction case, the spin excitation position C, as well as the spin correlations $\sigma_i^z \sigma_j^z$, relax to the stationary values at $T_0 \approx 10/J_0 = 500\,\text{ms}$. In the long-range interaction case, the observables first reach quasi-stationary (prethermal) values at a timescale T_0, and further relax to the stationary (thermal) values at a much longer timescale ($\sim 10^4 T_0$). The emergence of prethermalization in the long-range interaction case is signaled by a nonzero value of $\overline{C}$ at the intermediate timescale T_0. We can use $\overline{C}$ as an order parameter to characterize different dynamic behaviors. By continuously tuning the effective interaction range (indicated by the fitting parameter α) with the beatnote frequency μ, we find that (see figure 4) prethermalization only takes place when α is smaller than a critical value ($\alpha_C \approx 1.3$ for $N = 16$). For larger system size, the prethermalization–thermalization transition still occurs, but α_C becomes smaller and the transition becomes sharper. For the particular case $\alpha = 0$, the system has uniform coupling and its dynamics can be solved exactly. The exact solution shows that the system stays in the prethermal state forever with $\overline{C} = \frac{2}{N} - 1$ [33].

3. Mechanism of prethermalization and dynamic phase transition

We now give a physical explanation of why prethermalization and the variety of observed dynamic behaviors occur in this model. The distinctive short-time dynamics of $\langle \sigma_i^z(t) \rangle$
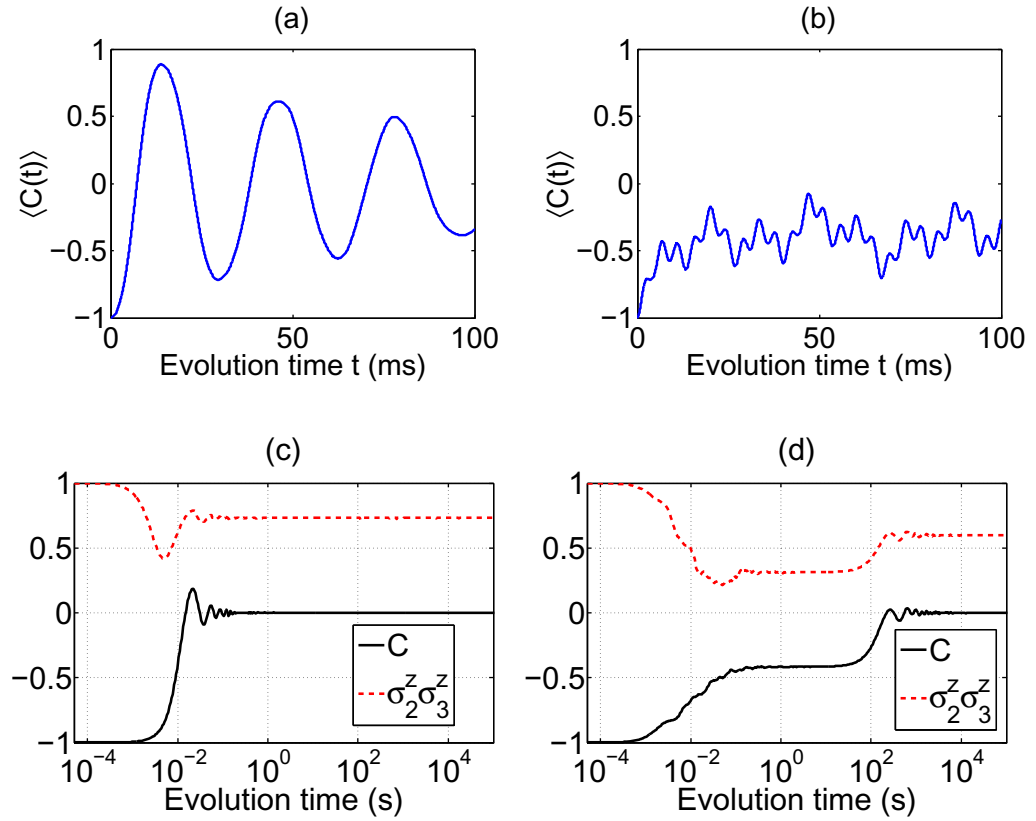
Figure 3. (a), (b) Short-time dynamics of σ_i^z and C for short-range (a) and long-range (b) interactions. (c), (d) Long-time dynamics of time-averaged C and $\sigma_i^z \sigma_j^z$ for (c) short-range and (d) long-range interactions. The parameters for the short-range and the long-range interactions are the same as in figure 2.

(figures 3(a) and (b)) can be explained by examining the energy spectrum of H_{XY} in the single spin excitation subspace (shown in figure 5(a)). In the short-range interaction case, the energy spectrum is close to linear. This is because H_{XY} can be roughly approximated with only neighboring interaction, and due to inhomogeneous lattice spacing, $\{J_{i,i+1}\}$ are similar to those in the 'quantum mirror' model [34, 35], resulting in a near dispersion-free spin wave propagation until nonlinearity sets in. On the other hand, the energy spectrum for the long-range interaction case is highly nonlinear, so the dynamics of the spin excitation is strongly dispersive.

The reason for a prethermal stage in the long-time dynamics, however, is much more complicated. Naively, the spin flip–flop matrix J_{ij} varies smoothly among sites for any $\alpha \in (0, 3)$, so the spin excitation should continuously diffuse from one end of the chain to the whole chain, and is not expected to get trapped somewhere in the middle for a long time. The two stage dynamics indicates that there are two different timescales implicit in the Hamiltonian, which is not at all obvious by looking at the J_{ij}. The time dynamics of any physical observable is simply given by

$$\langle A(t) \rangle = \sum_{m,n} \rho_{mn}(0) A_{nm}\, \mathrm{e}^{\mathrm{i}(E_m - E_n)t/\hbar},$$

where $\rho_{mn}(0)$ is the initial state's density matrix element in energy basis, the different timescales of the dynamics can be understood by computing the eigenenergy differences $\{E_m - E_n\}$, as
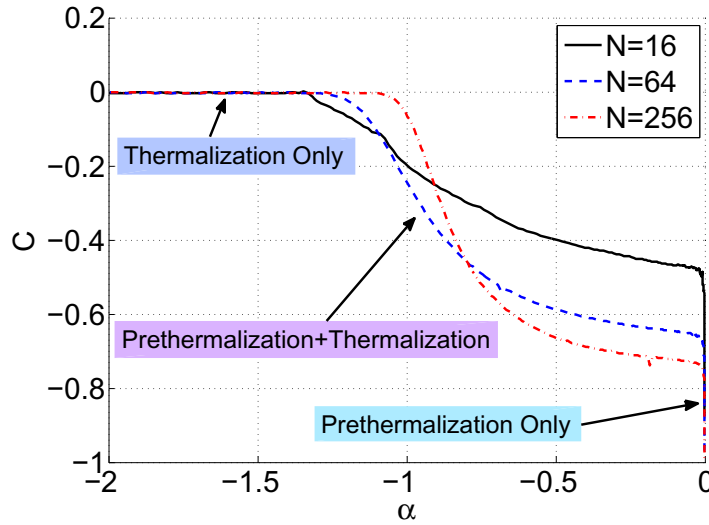
Figure 4. A dynamic 'phase diagram' with regard to the interaction range characterized by the fitting parameter α. The $N = 16$ case uses the parameters specified in figure 1, and the $N = 64$, $N = 256$ cases use the same parameters except that ω_z is scaled down by $\omega_z \propto \sqrt{\ln N}/N$ to maintain chain stability.

done in figure 5. In the short-range interaction case (figure 5(b)), all $\{E_m - E_n\}$ are continuously distributed from J_0 to $100J_0$, so a single-stage relaxation is expected after $T \sim T_0 = 10/J_0$. In the long-range interaction case (figure 5(c)), most $\{E_m - E_n\}$ still fall into the range of 1–$100J_0$, but there is a striking separate (i.e. gapped) branch at the much lower rate ($\sim 10^{-6}J_0$). This branch results from the near-degenerate pairs ($\{E_{2k} - E_{2k-1}\}$) of the eigenenergies (figure 5(a)) that make up the first half energy spectrum, and the number of these pairs scale up with system size N. Note that if we put the ions into a ring trap so that the lattice is translationally invariant, we find that there is no separate branch of the $\{E_m - E_n\}$ (figure 5(d)), and hence there is no prethermalization even with long-range interactions. The appearance of near-degenerate pairs $\{E_{2k} - E_{2k-1}\}$) in the spectrum of our model seems to arise from the combined effect of long-range interactions and inhomogeneous lattice spacing. Intuitively, from figure 2(b), the inhomogeneity causes the middle part of the chain to have smaller flip–flop interactions J_{ij} than the ends, potentially leading to a metastable state where the spin excitation is roughly localized in the left half of the chain. However, the existence of two distinct timescales is primarily due to the structure of the energy spectrum, which is not trivially related to inhomogeneity. We are still investigating if there is a wide class of inhomogeneous lattices that can give rise to similar dynamics.

Figure 5(e) shows that the thermal values can be well predicted by the DE, defined as

$$\rho_{\text{DE}} = \rho_{mn}(0)\delta_{mn}.$$

In the large N limit, under certain conditions implicit in the *eigenstate thermalization hypothesis* [3–5], the DE prediction will match the canonical ensemble prediction for thermalized states in classical statistical physics.
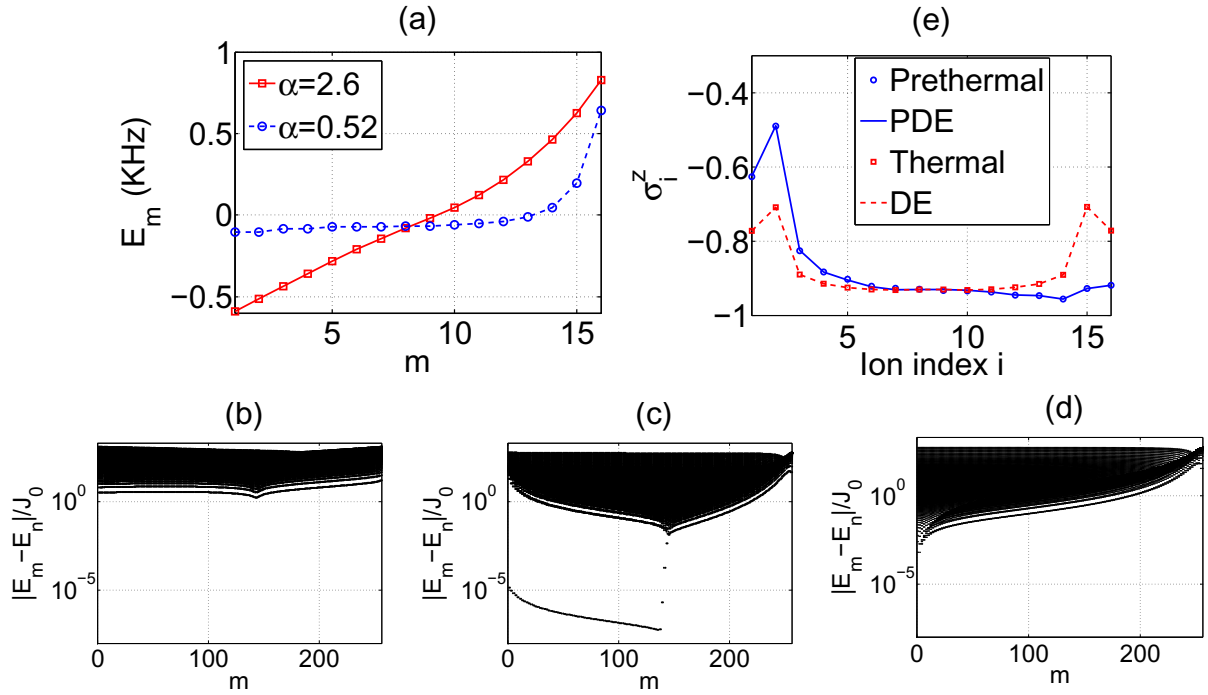
Figure 5. (a) Energy spectrum in the single spin excitation subspace for $N = 16$ spins with short and long-range interaction. (b)–(d) Scatter plot of the eigenenergy differences $\{E_m - E_n\}$ for $N = 256$ spins with (b) short-range interaction ($\alpha = 2.4$), (c) long-range interaction ($\alpha = 0.74$) and (d) long-range interaction ($\alpha = 0.74$) but with ions confined in a ring geometry with equal spacing. (e) Comparison of prethermal values of $\overline{\sigma_i^z}$ (blue circle, taken at $t = T_0 = 500$ ms) with partial diagonal ensemble (PDE) prediction (blue solid line) and thermal values (red square, taken at $t = 5 \times 10^3 s$) with diagonal ensemble (DE) prediction (red dashed line) based on long-range interaction pattern J_{ij} shown in figure 2(b).

As prethermalization is due to an emergent small scale of energy differences in the Hamiltonian, to predict the prethermal values here, we can define the PDE:

$$\rho_{\text{PDE}} = \begin{cases} \rho_{mn}(0)\delta_{mn}, & |\nu_m - \nu_n| \gtrsim 1/T_0, \\ \rho_{mn}(0), & |\nu_m - \nu_n| \ll 1/T_0, \end{cases} \tag{3}$$

where $\{\nu_m\}$ are the eigenenergies. We find that the PDE can accurately predict the prethermal values of local observables $\overline{\sigma_i^z}$, as shown in figure 5(d). Roughly speaking, the prethermalization timescale is determined by the average level spacing ($\sim 10/J_0$), and the thermalization timescale is determined by the minimum level spacing ($\sim 10^4/J_0$ as in figure 5(d)).

The dynamic phase transition can be associated with breaking of the lattice inversion (parity) symmetry, reminiscent of symmetry breaking in the equilibrium phase transitions. Our Hamiltonian H_{XY} is symmetric under the space inversion around $z = 0$ (figure 1), but we start from an initial state that does not have this symmetry. The thermal state, with no memory of the initial state, is described by the diagonal ensemble ρ_{DE} and restores this symmetry as $\overline{C} = 0$. However, the prethermal state does not restore the Hamiltonian symmetry due to its non-zero

$\overline{C}$ value, which indicates that some 'memory' of the initial state is preserved in the prethermal state. The intermediate timescale T_0 for observation of the prethermal state gives a microscopic interpretation of why this state can break the parity symmetry: one cannot distinguish the near-degenerate pairs of eigenstates in the energy spectrum, so linear combinations within each pair are allowed. Since the two eigenstates of the pair have either even or odd parity, their linear combinations can break the parity symmetry. The dynamic phase diagram shown in figure 4 also has the hint of two non-analytical points: one is where $\overline{C}$ becomes non-zero, representing the appearance of prethermalization, and the other is where $\overline{C}$ approaches $\frac{2}{N} - 1$ ($\alpha \rightarrow 0$), representing the disappearance of thermalization. Note that the thermodynamic limit of our system is not well defined, as to keep a linear ion chain stable, the length of the chain L cannot be kept proportional to N as N becomes large. Thus, it is not clear if a dynamical phase transition point can be obtained in some generalized thermodynamic limit (we are also limited by a finite number of lattice sites that can be studied using our numerical methods).

4. Discussion of experimental detection and summary

The transverse field Ising Hamiltonian equation (1) has already been experimentally simulated in [19] for the $N = 16$ ions, and highly efficient *in situ* measurement of spin polarization (σ_i^z) and spin correlation ($\sigma_i^z \sigma_j^z$) has been demonstrated. The XY Hamiltonian (equation (2)) can thus be readily obtained by turning up the effective transverse magnetic field. The non-equilibrium initial state preparation requires a focused laser beam, but is relatively easy due to the large ion spacing near the ends. The laser power and trap frequencies used for generating the interaction pattern J_{ij} shown in figure 2 are within current experimental reach [17, 19]. The observation of prethermalization and the dynamic phase transition shown in figures 3 and 4 only requires the spin decoherence time to be longer than $T_0 = 10/J_0 = 500$ ms, and coherence times of up to 2.5 s have been experimentally achieved by using the hyperfine qubit of Yb$^+$ ions [36]. However, the second stage of thermalization for the long-range interaction case requires much longer times, and is beyond current experimental reach, similar to the experiment on prethermalization using cold atoms in [14].

In summary, we have proposed a novel scheme to observe a peculiar prethermalization phenomenon and dynamic phase transitions in a trapped ion quantum simulator. The required conditions can be realized by using current experimental technology. We provide an explanation of the mechanism of prethermalization and the dynamic phase transition in our proposed model. We believe that the wealth of interesting dynamic properties for a system with continuously tunable range of interactions is far from exhausted.

Note Added: After completion of this work, we became aware of [37], in which similar local quench dynamics yields results consistent with the work presented here on the short-time behavior of small versus large α power law interaction, and [38], which studies entanglement growth following a global quench of the Hamiltonian given by equation (1) under different α.

IOP Institute of Physics Φ DEUTSCHE PHYSIKALISCHE GESELLSCHAFT

References

[1] Polkovnikov A, Sengupta K, Silva A and Vengalattore M 2011 Colloquium: nonequilibrium dynamics of closed interacting quantum systems *Rev. Mod. Phys.* **83** 863

[2] Cazalilla M A and Rigol M 2010 Focus on dynamics and thermalization in isolated quantum many-body systems *New J. Phys.* **12** 055006

[3] Deutsch J M 1991 Quantum statistical mechanics in a closed system *Phys. Rev.* A **43** 2046

[4] Srednicki M 1994 Chaos and quantum thermalization *Phys. Rev.* E **50** 888

[5] Rigol M, Dunjko V and Olshanii M 2008 Thermalization and its mechanism for generic isolated quantum systems *Nature* **452** 854–8

[6] Rigol M, Dunjko V, Yurovsky V and Olshanii M 2007 Relaxation in a completely integrable many-body quantum system: an *ab initio* study of the dynamics of the highly excited states of 1D lattice hard-core bosons *Phys. Rev. Lett.* **98** 050405

[7] Reimann P 2008 Foundation of statistical mechanics under experimentally realistic conditions *Phys. Rev. Lett.* **101** 190403

[8] Masanes L, Roncaglia A J and Acín A 2013 Complexity of energy eigenstates as a mechanism for equilibration *Phys. Rev.* E **87** 032137

[9] Brandão F G S L, Cwikliński P, Horodecki M, Horodecki P, Korbicz J K and Mozrzymas M 2012 Convergence to equilibrium under a random Hamiltonian *Phys. Rev.* E **86** 031101

[10] Reimann P and Kastner M 2012 Equilibration of isolated macroscopic quantum systems *New J. Phys.* **14** 043020

[11] Gong Z-X and Duan L-M 2011 Comment on 'Foundation of statistical mechanics under experimentally realistic conditions' arXiv:1109.4696

[12] Kinoshita T, Wenger T and Weiss D S 2006 A quantum Newton's cradle *Nature* **440** 900–3

[13] Trotzky S, Chen Y-A, Flesch A, McCulloch I P, Schollwöck U, Eisert J and Bloch I 2012 Probing the relaxation towards equilibrium in an isolated strongly correlated one-dimensional Bose gas *Nature Phys.* **8** 325–30

[14] Gring M, Kuhnert M, Langen T, Kitagawa T, Rauer B, Schreitl M, Mazets I, Adu Smith D, Demler E and Schmiedmayer J 2012 Relaxation and prethermalization in an isolated quantum system *Science* **337** 1318–22

[15] Friedenauer A, Schmitz H, Glueckert J T, Porras D and Schaetz T 2008 Simulating a quantum magnet with trapped ions *Nature Phys.* **4** 757–61

[16] Kim K, Chang M-S, Korenblit S, Islam R, Edwards E E, Freericks J K, Lin G-D, Duan L-M and Monroe C 2010 Quantum simulation of frustrated Ising spins with trapped ions *Nature* **465** 590–3

[17] Islam R *et al* 2011 Onset of a quantum phase transition with a trapped ion quantum simulator *Nature Commun.* **2** 377

[18] Britton J W, Sawyer B C, Keith A C, Joseph Wang C-C, Freericks J K, Uys H, Biercuk M J and Bollinger J J 2012 Engineered two-dimensional Ising interactions in a trapped-ion quantum simulator with hundreds of spins *Nature* **484** 489–92

[19] Islam R, Senko C, Campbell W C, Korenblit S, Smith J, Lee A, Edwards E E, Wang C-C J, Freericks J K and Monroe C 2013 Emergence and frustration of magnetism with variable-range interactions in a quantum simulator *Science* **340** 583–7

[20] Schneider Ch, Porras D and Schaetz T 2012 Experimental quantum simulations of many-body physics with trapped ions *Rep. Prog. Phys.* **75** 024401

[21] Berges J, Borsányi Sz and Wetterich C 2004 Prethermalization *Phys. Rev. Lett.* **93** 142002

[22] Kollar M, Alexander Wolf F and Eckstein M 2011 Generalized Gibbs ensemble prediction of prethermalization plateaus and their relation to nonthermal steady states in integrable systems *Phys. Rev.* B **84** 054304

[23] Barnett R, Polkovnikov A and Vengalattore M 2011 Prethermalization in quenched spinor condensates *Phys. Rev.* A **84** 023606

[24] van den Worm M, Sawyer B C, Bollinger J J and Kastner M 2013 Relaxation timescales and decay of correlations in a long-range interacting quantum simulator *New J. Phys.* **15** 083007

[25] Heyl M, Polkovnikov A and Kehrein S 2013 Dynamical quantum phase transitions in the transverse-field Ising model *Phys. Rev. Lett.* **110** 135704

[26] Kim K, Chang M-S, Islam R, Korenblit S, Duan L-M and Monroe C 2009 Entanglement and tunable spin–spin couplings between trapped ions using multiple transverse modes *Phys. Rev. Lett.* **103** 120502

[27] Emch G G 1966 Non-Markovian model for the approach to equilibrium *J. Math. Phys.* **7** 1198–206

[28] Radin C 1970 Approach to equilibrium in a simple model *J. Math. Phys.* **11** 2945–55

[29] Kastner M 2011 Diverging equilibration times in long-range quantum spin models *Phys. Rev. Lett.* **106** 130601

[30] Korenblit S *et al* 2012 Quantum simulation of spin models on an arbitrary lattice with trapped ions *New J. Phys.* **14** 095024

[31] Rigol M, Muramatsu A and Olshanii M 2006 Hard-core bosons on optical superlattices: dynamics and relaxation in the superfluid and insulating regimes *Phys. Rev.* A **74** 053616

[32] Ponomarev A V, Denisov S and Hänggi P 2011 Thermal equilibration between two quantum systems *Phys. Rev. Lett.* **106** 010405

[33] Sciolla B and Biroli G 2011 Dynamical transitions and quantum quenches in mean-field models *J. Stat. Mech.* **2011** 11003

[34] Albanese C, Christandl M, Datta N and Ekert A 2004 Mirror inversion of quantum states in linear registers *Phys. Rev. Lett.* **93** 230502

[35] Yao N Y, Gong Z-X, Laumann C R, Bennett S D, Duan L-M, Lukin M D, Jiang L and Gorshkov A V 2013 Quantum logic between remote quantum registers *Phys. Rev.* A **87** 022306

[36] Olmschenk S, Younge K C, Moehring D L, Matsukevich D N, Maunz P and Monroe C 2007 Manipulation and detection of a trapped Yb^+ hyperfine qubit *Phys. Rev.* A **76** 052314

[37] Hauke P and Tagliacozzo L 2013 Spread of correlations in long-range interacting systems *Phys. Rev. Lett.* **111** 207202

[38] Schachenmayer J, Lanyon B P, Roos C F and Daley A J 2013 Entanglement growth in quench dynamics with variable range interactions *Phys. Rev.* X **3** 031015